Phys. Status Solidi B **248**, No. 7, 1718–1722 (2011) / **DOI** 10.1002/pssb.201046596

physica status solidi b
www.pss-b.com
basic solid state physics

Avalanche-like electric-field-induced photocurrent gain in resonant tunneling hydrogenated nanocrystalline silicon system

Jing Chen*[,1], Jia Jia Lu[2], Rong Zhang[2], Yong Sheng Liu[1], and Wen Zhong Shen[2]

[1] Department of Physics and Mathematics, Shanghai University of Electric Power, 201300 Shanghai, P.R. China
[2] Department of Physics, Shanghai Jiaotong University, 200240 Shanghai, P.R. China

Received 25 November 2010, revised 28 January 2011, accepted 31 January 2011
Published online 28 February 2011

Keywords nanostructures, photocurrent, resonant tunneling, Si

* Corresponding author: e-mail jingchen@shiep.edu.cn, Phone: +86 021 13371897027, Fax: +86 021 68070264

By introducing photogeneration into the rate equation of the two-energy-level system, we obtain the photocurrent gain effect theoretically in hydrogenated nanocrystalline silicon (nc-Si:H) structure, which is consistent with the reported experimental data. To understand the carrier-transport characteristics in such nanostructures, the time-dependent distributions of the electric field and photocurrent inside nc-Si:H structure at different absorption coefficients have been calculated. The result shows that the occurrence of photocurrent enhancement is accompanied by an avalanche-like phenomenon of the electric field during its dynamic process to achieve equilibrium. Further investigation reveals that the physical nature behind this photocurrent gain lies in the existence of the resonant tunneling inside the nc-Si:H structure.

© 2011 WILEY-VCH Verlag GmbH & Co. KGaA, Weinheim

1 Introduction Studies of photocurrent in low-dimensional systems have attracted considerable interests due to their particular characteristics aroused by the quantum confinement effect [1–4]. Having knowledge of the photoelectric nature inside these systems will be essential to realize the design of low-dimensional-material-based optoelectronic devices. In the past decades, much more attention have been paid on the hydrogenated nanocrystalline silicon (nc-Si:H) thin films because of their importance in fundamental physics and potential applications to optoelectronic devices, e.g., optical memories, solar cells, and single electron transistors [5, 6]. Further, the current–voltage characteristics have been carried out at different external conditions experimentally. Some interesting phenomena related to the quantum tunneling effect were observed in nc-Si:H heterostructures at low temperature, such as periodical negative differential conductivity [7].

Recently, we have reported the temperature-dependent photocurrent performance of nc-Si:H thin-film samples [8]. Detailed analyses have been carried out on the exploring of the two main photocurrent peaks. In addition, there is another interesting photocurrent gain phenomenon observed at about 1.20 eV, as shown in Fig. 2 of Ref. [8]. Though this gain effect is relatively weak, its dependency on the photon energy as well as the temperature clearly demonstrates the existence of some unclear underlying physical mechanisms. In our previous paper, we basically ruled out the possibility of the optical phonon absorption-induced enhancement, and expressed a preliminary viewpoint that this photocurrent gain may be caused by the formation of discrete energy levels inside the nc-Si:H structure. However, the root cause is still unclear. Therefore, further studies, particularly theoretical investigation is necessary for this observation.

So far, several theoretical models concerning the photoelectric conversion and carrier transport in nanostructures have been reported [9–12]. Most of them only consider one quantum level inside their systems. As a result, it is lack of the resonant tunneling in those models that may be a key approach for the carriers transport in nanostructures, especially at very low temperature. Thus, it is essential to establish a model that involves the resonant tunneling process. In this report, we have proposed a modified rate equation of two-energy-level system to simulate the photocurrent of nc-Si:H thin film. A gain phenomenon has been obtained theoretically, which is in accordance with the experimental observation. Through detailed analyses of the time-dependent distribution of the electric field and photocurrent inside the nc-Si:H structure, the physical mechanism behind this special gain effect is revealed.

© 2011 WILEY-VCH Verlag GmbH & Co. KGaA, Weinheim

2 Results and discussion Figure 1 gives the observed temperature-dependent photocurrent spectra of the studied sample with photon energy in the range of 1.1–1.4 eV. The detailed information of the growth and structural characteristics of the studied nc-Si:H sample, and the photocurrent experimental setup can be seen in Refs. [8, 13]. The main peak centered about 1.25 eV is considered as originating from the photogenerated carriers in the nc-Si:H thin film [8]. Due to the thermalization effect, the photocurrent decreases with photon energy on the high-energy side. However, more attention should be paid to the low-energy side of the main peak, where a gain effect near 1.20 eV is observed, accompanying the enhancement of photocurrent when the photon energy is larger than 1.20 eV. This phenomenon becomes blurred on increasing the temperature and finally disappears at $T = 300$ K, as shown in Fig. 1.

To represent our nc-Si:H sample, we consider an ideal structure as indicated in Fig. 2a, where the c-Si nanodots with uniform size are orderly arranged and surrounded by the a-Si. Due to the field-induced localization, three-dimensional quantum confinement in the nanodots may turn into one-dimensional confinement along the electric-field direction [14]. Hence, the electronic energy band diagram of nc-Si:H can be assumed as N c-Si wells of width W coupled by a-Si barriers, where the height of the barrier is equal to the conduction band discontinuity of c-Si and a-Si. Calculation shows that two energy levels are confined in the c-Si well. Thus, the theoretical model proposed to simulate the above observation should be considered for a two-energy-level system.

Our simulation is based on a modified rate equations [15]. Inside each c-Si well, we will consider two discrete quantum levels. In the kth nanodot layer, the electron densities of the two levels are denoted as n_1^k and n_2^k. If given a certain condition, n_1^k and n_2^k will change until they both arrive at a dynamic equilibrium. Here, *e.g.*, n_1^k has eight mechanisms to be altered as designated in Fig. 2b: (1) intersubband relaxation $n_2^k \to n_1^k$, (2) miniband transport $n_1^{k-1} \to n_1^k$, (3) miniband transport $n_1^k \to n_1^{k+1}$, (4) and (5) resonant tunneling $n_1^k \leftrightarrow n_2^{k+1}$, (6) and (7) resonant tunneling

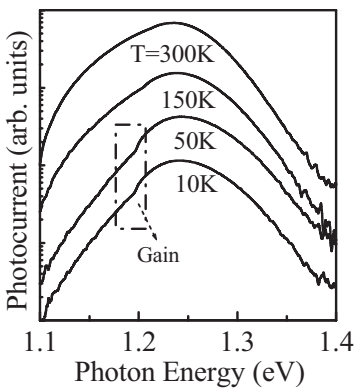

Figure 1 Photocurrent spectra of nc-Si:H sample with photon energy in the range of 1.1–1.4 eV at different temperatures.

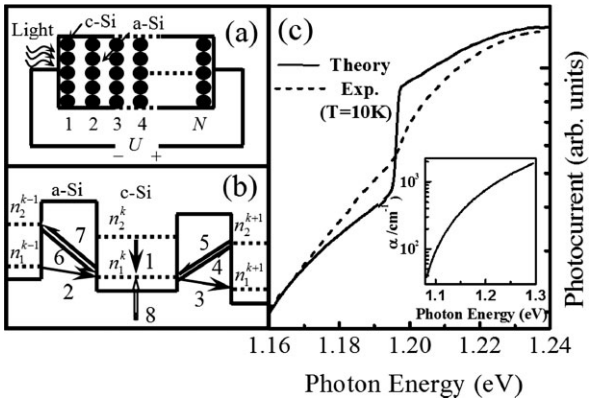

Figure 2 (a) Schematic diagram of the studied nc-Si:H sample. (b) Conduction band diagram of nc-Si:H with an applied bias. The eight channels that n_1^k in the kth layer changes through are designated. (c) Calculated (solid curve) and experimental (dashed curve) photocurrent with the photon energy from 1.16 to 1.24 eV, the inset is the extracted absorption coefficient of the nc-Si:H sample dependent on the photon energy.

$n_2^{k-1} \leftrightarrow n_1^k$, (8) photon-generated electron. Thus, the total electron rate equations in the kth layer are:

$$\begin{aligned}\dot{n}_1^k &= A^k + n_1^{k-1}R_{\mathrm{MB1}}(E^k) + n_2^{k-1}P_{2\to 1'}(-E^k) \\ &\quad + n_2^{k+1}P_{1\leftarrow 2'}(E^{k+1}) - n_1^k\big(P_{1\to 2'}(E^{k+1}) \\ &\quad + P_{2\leftarrow 1'}(-E^k) + R_{\mathrm{MB1}}(E^{k+1})\big) + G(\lambda, z),\end{aligned} \tag{1a}$$

$$\begin{aligned}\dot{n}_2^k &= -A^k + n_2^{k-1}R_{\mathrm{MB2}}(E^k) + n_1^{k-1}P_{1\to 2'}(E^k) \\ &\quad + n_1^{k+1}P_{2\leftarrow 1'}(-E^{k+1}) - n_2^k\big(P_{2\to 1'}(-E^{k+1}) \\ &\quad + P_{1\leftarrow 2'}(E^k) + R_{\mathrm{MB2}}(E^{k+1})\big), \\ &\quad (k = 1, \ldots, N),\end{aligned} \tag{1b}$$

where A^k is the rate of intersubband relaxation, E^k the electric field on the barrier of the kth layer, $R_{\mathrm{MB}i}(E^k)$ ($i = 1$ or 2) the miniband transport relaxation rate, $P_{i\leftrightarrow i'}(E^k)$ the resonant tunneling probability, and $G(\lambda,z)$ is the electron–hole generation rate at a depth z inside the structure for the incident light with the wavelength of λ:

$$G(\lambda, z) = \alpha(\lambda)F_0(\lambda)\exp(-\alpha(\lambda)z), \tag{2}$$

where $\alpha(\lambda)$ is the light absorption coefficient, $F_0(\lambda)$ is the number of photons per second hitting per unit of area on the structure.

It should be noted that all the rates are dependent on the electric field E^k. Then, the current density transport from the kth to the $(k+1)$th well is:

$$j^k(E^k) = j_{\mathrm{MB}}^k(E^k) + j_{\mathrm{RT}}^k(E^k), \tag{3}$$

where $j_{\mathrm{MB}}^k(E^k)$ and $j_{\mathrm{RT}}^k(E^k)$ represent the miniband transport and resonant tunneling current density respectively, which

© 2011 WILEY-VCH Verlag GmbH & Co. KGaA, Weinheim

can be expressed as:

$$j^k_{\mathrm{MB}}\left(E^k\right) = eW\left[n^k_1 R_{\mathrm{MB1}}\left(E^k\right) + n^k_2 R_{\mathrm{MB2}}\left(E^k\right)\right], \quad (4a)$$

$$j^k_{\mathrm{RT}}\left(E^k\right) = eW\left[n^k_1 P_{1\to 2'}\left(E^{k+1}\right) + n^k_2 P_{2\to 1'}\left(-E^{k+1}\right) - n^{k+1}_1 P_{2\to 1'}\left(-E^{k+1}\right) - n^{k+1}_2 P_{1\leftarrow 2'}\left(E^{k+1}\right)\right]. \quad (4b)$$

Here, e is the charge on the electron. The results obtained from solving the above model are better illustrated by means of a numerical method, where the number of nanodot layers is assumed $N = 30$ and the bias added to the structure is $U = 1$ V. We first suppose a uniform field distribution, with which the initial n^k_i can be obtained. Then, we apply a Runge–Kutta procedure to Eqs. (1a) and (1b), until all rates $\dot{n}^k_i$ become smaller than a threshold value, which indicates a steady state has been established. Thus, the final electric-field distribution and the photocurrent can be calculated.

Figure 2c gives the simulated photocurrent (solid curve) of nc-Si:H with the photon energy from 1.16 to 1.24 eV. Similarly, the photocurrent gain effect at about 1.20 eV is obtained. It is consistent with the observations at low temperature of 10 K, as also plotted by the dashed curve in the figure. One may argue that the gain in the experimental data is much more moderate than the theoretical one. The reason is that we have ignored the discrimination originated from the electron thermal effect of the sample, since it is too weak at very low temperature, leaving the discussion and conclusion below still valid.

Calculation shows that the photocurrent changes with the photon energy mainly due to the variation of absorption coefficient at different photon energy. In the inset of Fig. 2c, we plot the absorption coefficient $\alpha(\lambda)$ used in our model, which was extracted from the experimental transmission data [16]. When the photon energy varies from 1.16 to 1.24 eV, the α of nc-Si:H increases monotonically from 400 to 1200 cm^{-1}. In addition, it has a more rapid increment compared to the absorption process of c-Si in the same energy range. This is due to the enlarged surface-to-volume ratio in nc-Si:H, improving the optical absorption cross section.

Although Fig. 2c reveals that we can fit the experimental result, the downside is that the sample is viewed as a black-box device, only collected current flowing out of the structure was measured. In order to obtain the in-depth information of the photogenerated electron transport, which is critical to understand the gain phenomenon, it is necessary to calculate the distribution of photocurrent density throughout the structure.

The calculated distribution of photocurrent density j^k inside the nc-Si:H structure at steady state is given in Fig. 3. It is interesting to find that the performance of j^k splits into two parts. As α increases from 400 to 700 cm^{-1}, j^1 decreases, while j^{30} increases, that is, the slope of j dependency on the nanodot layer gradually increases. When α further rises to 800 cm^{-1}, the photocurrent has an increasing step. And then again slowly changes the slope as the absorption coefficient

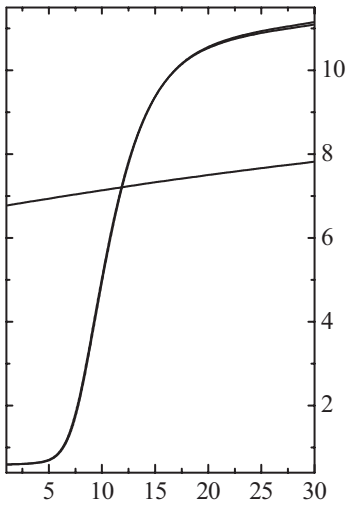

in the range of 800–1200 cm^{-1}. Similar characteristics are also exhibited in the distribution of electric field E^k (together shown in Fig. 3). As α increases from 400 to 700 cm^{-1}, the slope of E^k with nanodot layer increases. Whereas α is larger than 800 cm^{-1}, the shape of the electric-field distribution changes greatly. Most obviously, the electric field E^k in the first several layers drops approximately to zero, and then increases quickly along the layers.

It is found that the different behavior of photocurrent and electric-field distribution with changing absorption coefficient just corresponds to the experimental observed current gain according to the inset of Fig. 2c. On the basis of the description of Fig. 3, the general view of the absorption coefficient influence on the photocurrent can be obtained as follows: When increasing the absorption coefficient, the number of photons absorbed by the nc-Si:H material rises correspondingly, resulting in higher electron concentration, breaking the initial dynamic equilibrium. Due to the Gauss law, we get $(E^{k+1}-E^k)\propto(n^k_1+n^k_2)$, thus $(E^{k+1}-E^k)$ increases. Since the applied external bias is fixed, the slope of electric fields on the nanodot layers will increase, which will affect the resonant tunneling probability. As a result, the resonant tunneling current changes, thereby altering the total photocurrent. On the other hand, the variation of photocurrent will in turn influence the distribution of the electron density, which may once again require the adjustment of the electric field. And so on, until a new dynamic equilibrium is eventually established.

We know that at very low temperatures, the collected photocurrent may be dominated by the tunneling current, while the resonant tunneling probability is impacted by the electric field. According to our previous discussion and simulation results, we find that the higher the absorption coefficient, the larger the electric field on the last nanodot,

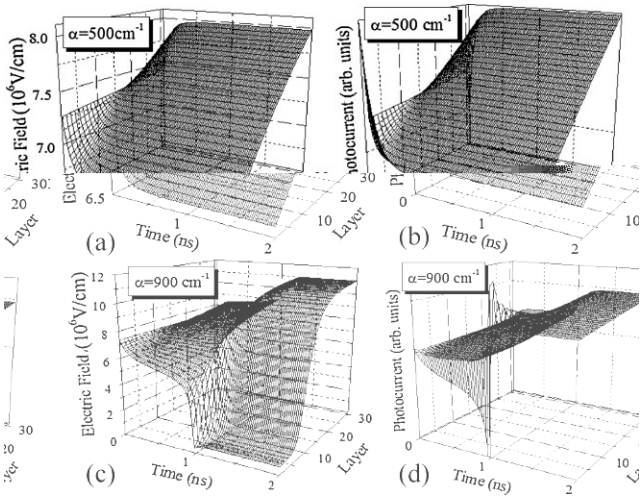

Figure 4 The simulated time dependence of (a) the electric field at $\alpha = 500\,\mathrm{cm}^{-1}$, (b) photocurrent density at $\alpha = 500\,\mathrm{cm}^{-1}$, (c) the electric field at $\alpha = 900\,\mathrm{cm}^{-1}$, and (d) photocurrent density at $\alpha = 900\,\mathrm{cm}^{-1}$.

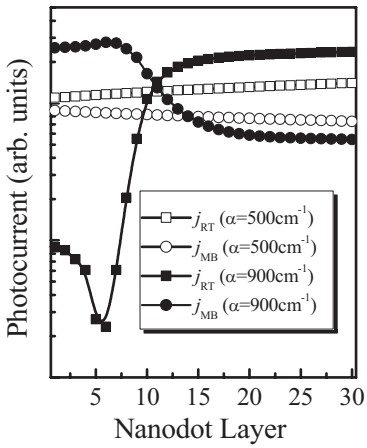

Figure 5 The distribution of resonant tunneling current and miniband transport current components at steady state with $\alpha = 500$ and $900\,\mathrm{cm}^{-1}$, respectively.

and the larger the photocurrent flowing out of the nc-Si:H structure. Nevertheless, it is still not clear for the different behavior of photocurrent as well as electric field between the absorption coefficient in the range of 400–700 cm^{-1} and 800–1200 cm^{-1}. In Fig. 4, we give the time-dependent electric field and photocurrent distribution inside the structure. For comparison, the absorption coefficient is selected as $\alpha = 500$ and $900\,\mathrm{cm}^{-1}$, respectively, to represent the different behavior described previously.

The calculated time-dependent electric field and photocurrent density distribution throughout the whole structure for $\alpha = 500\,\mathrm{cm}^{-1}$ are shown in Figs. 4a and b. Starting from the initial state, the distribution of the electric field adjusts continuously and becomes stable within 0.5 ns. A similar trend is also reflected in the distribution of photocurrent. Here, more attention should be paid to the first several nanodot layers, where the electric field decreases smoothly with time, meanwhile the photocurrent density also deduces until it reaches the stable state. The dynamic process for $\alpha = 900\,\mathrm{cm}^{-1}$ is shown in Figs. 4c and d, which exhibits different time evolutions compared with those at $\alpha = 500\,\mathrm{cm}^{-1}$. In particular, for the former nanodot layers, the electric field decreases gradually with time at first, afterward it experiences a sharp reduction to nearly zero, and then it achieves equilibrium. While for the photocurrent, it first reduces, and then undergoes a dramatic increment before finally reaching a stable state.

The above discussion shows that the biggest discrimination between the time-dependent photocurrent and electric-field behavior at different absorption coefficient conditions is that they both experience a course of two adjustments for the case of $\alpha = 900\,\mathrm{cm}^{-1}$ compared with those of $\alpha = 500\,\mathrm{cm}^{-1}$. Moreover, the second adjustment of electric field reveals an avalanche-like phenomenon for the former nanodot layers. With the quick decrement of the electric field, the probability of resonant tunneling reduces and correspondingly the tunneling current will decrease. On the contrary, we note that the photocurrent increases in these layers, which means that the miniband transport current increases greatly and becomes the dominant component of the photocurrent. Figure 5 displays the calculated resonant tunneling current j_{RT} and miniband transport current j_{MB} components separately at steady state throughout the whole structure for $\alpha = 500$ and $900\,\mathrm{cm}^{-1}$. It is clear that when $\alpha = 900\,\mathrm{cm}^{-1}$, j_{RT} is much smaller than j_{MB} in the first nanodot layer. And along with the nanodot layer, j_{RT} first decreases and then increases, whereas j_{MB} has the opposite trend. When k is larger than 10, j_{RT} starts to be higher than j_{MB} and becomes the dominant part in the final collected photocurrent. While for the case of $\alpha = 500\,\mathrm{cm}^{-1}$, j_{RT} is higher than j_{MB} throughout the whole structure.

With regard to the avalanche-like phenomenon of electric field at $\alpha = 900\,\mathrm{cm}^{-1}$, we consider it as a result of electric-field-dependent resonant tunneling behavior. During the process of dynamic adjustments, the tunneling probability will be greatly reduced if E decreases to a certain value, leading to the dramatic reduction of tunneling current. In order to maintain the dynamic electron concentration, the miniband transport current has to be enhanced, which will be realized by sharply increasing the electron concentration in the layers since the miniband transport coefficient is not subject to the electric field. Meanwhile, the substantial increment of electron concentration again breaks the distribution of electric field, resulting in a rapid decrement of electric field based on the Gauss law.

Therefore, the gain effect of the observed photocurrent originates from the avalanche-like second adjustment of electric field when it reduces to a critical value during the dynamic process. In this case, the critical condition comes from the absorption process. That is, on increasing the absorption coefficient, more photoelectrons are generated. When the electron density reaches a certain level, it will lead

© 2011 WILEY-VCH Verlag GmbH & Co. KGaA, Weinheim

to a different dynamic behavior for the electric field and photocurrent. However, it is important to note that the absorption coefficient variation caused by different incident photon energy is only an external cause, while the nature lies on the existence of resonant tunneling effect due to the discrete levels in nc-Si:H material, which enables the complementarity between the resonant tunneling current and miniband transport current. Especially in the first several nanodot layers, the second adjustment is accompanied with a conversion of photocurrent component from resonant tunneling dominant to miniband transport dominant.

3 Conclusions In summary, we observe a photocurrent gain effect in the nc-Si:H sample at low temperature, which can be simulated by a modified rate equation of a two-energy-level system. By employing the theoretical model, we calculate the absorption-coefficient-dependent distributions of electric field and photocurrent. It is found that their behavior has a split between different absorption coefficient regions. Detailed analyses reveal that an avalanche-like phenomenon of the electric field appears during the dynamic process of achieving equilibrium, accompanied by the conversion of resonant tunneling dominant current to the miniband transport-dominant current, which leads to the observed enhancement of total photocurrent. However, the physical nature behind the gain effect is the resonant tunneling effect due to the discrete quantum energy levels inside the nc-Si:H sample.

Acknowledgements This work was supported by the "Chen Guang" project sponsored by the Shanghai Municipal Education Commission and the Shanghai Education Development Foundation (Grant No. 2008CG60), the National Natural Science Foundation of China (Grant No. 10804072).

References

[1] I. Mukhametzhanov, Z. H. Chen, O. Baklenov, E. T. Kim, and A. Madhukar, Phys. Status Solidi B **224**, 697 (2001).
[2] S. K. Kim, B. H. Kim, C. H. Cho, and S. J. Park, Appl. Phys. Lett. **94**, 183106 (2009).
[3] A. Maharjan, K. Pemasiri, P. Kumar, A. Wade, L. M. Smith, H. E. Jackson, J. M. Yarrison-Rice, A. Kogan, S. Paiman, Q. Gao, H. H. Tan, and C. Jagadish, Appl. Phys. Lett. **94**, 193115 (2009).
[4] E. Antolín, A. Martí, C. R. Stanley, C. D. Farmer, E. Cánovas, N. López, P. G. Linares, and A. Luque, Thin Solid Films **516**, 6919 (2008).
[5] X. J. Hao, E. C. Cho, C. Flynn, Y. S. Shen, S. C. Park, G. Conibeer, and M. A. Green, Sol. Energy Mater. Sol. Cells **93**, 273 (2009).
[6] X. Y. Chen and W. Z. Shen, Appl. Phys. Lett. **85**, 287 (2004).
[7] J. Chen, J. J. Lu, W. Pan, K. Zhang, X. Y. Chen, and W. Z. Shen, Nanotechnology **18**, 015203 (2007).
[8] R. Zhang, X. Y. Chen, J. J. Lu, and W. Z. Shen, J. Appl. Phys. **102**, 123708 (2007).
[9] A. Luque and A. Martí, Phys. Rev. Lett. **78**, 5014 (1997).
[10] J. L. Wang and E. X. Wu, Chin. Phys. B **16**, 848 (2007).
[11] V. Aroutiounian, S. Petrosyana, and A. Khachatryan, Sol. Energy Mater. Sol. Cells **89**, 165 (2005).
[12] S. Tomic, T. S. Jones, and N. M. Harrison, Appl. Phys. Lett. **93**, 263105 (2008).
[13] X. Y. Chen, W. Z. Shen, and Y. L. He, J. Appl. Phys. **97**, 024305 (2005).
X. Y. Chen and W. Z. Shen, Phys. Rev. B **72**, 035309 (2005).
[14] Q. Y. Ye, R. Tsu, and E. H. Nicollian, Phys. Rev. B **44**, 1806 (1991).
[15] F. Prengel, A. Wacker, and E. Scholl, Phys. Rev. B **50**, 1705 (1994).
[16] R. Zhang, X. Y. Chen, K. Zhang, and W. Z. Shen, J. Appl. Phys. **100**, 104310 (2006).

© 2011 WILEY-VCH Verlag GmbH & Co. KGaA, Weinheim